EARTHQUAKE ENGINEERING AND STRUCTURAL DYNAMICS, VOL. 13, 173–193 (1985)

DISPLACEMENT SOLUTIONS FOR DYNAMIC LOADS IN TRANSVERSELY-ISOTROPIC STRATIFIED MEDIA

G. WAAS, H. R. RIGGS AND H. WERKLE

Hochtief AG, Abt. KTI, Bockenheimer Landstr. 24, 6000 Frankfurt/Main 1, West Germany

SUMMARY

Solutions for the displacements caused by dynamic loads in a viscoelastic transversely-isotropic medium are derived. The medium extends horizontally to infinity, but is bounded below by a rigid base. Stratification of the medium presents no difficulties. The medium is discretized in the vertical direction only; discretization in the horizontal direction is obviated by use of analytical solutions to the equations of motion.

Application of the displacement solutions to soil–structure interaction is illustrated. A soil flexibility matrix (and hence, a stiffness matrix) for a surface foundation follows directly from the displacement solutions. A simple modification to obtain the soil stiffness for an embedded foundation of arbitrary geometry is described. Stiffnesses of rigid surface and embedded foundations are computed and compared with previously published results. In addition, the dynamic stiffness of a rigid surface foundation on a soil layer with linearly increasing shear modulus is compared to that for a homogeneous soil layer. A reduction in radiation damping is found to result from the inhomogeneity.

INTRODUCTION

Solutions for the displacements caused by static and dynamic loads acting in a layered medium have many applications in geomechanics and seismology. Of particular interest here are applications in the area of soil–structure interaction. Specifically, such solutions can be used to compute the stiffness of the soil foundation. This stiffness then can be used in conjunction with the structure stiffness in the determination of structural response to loads on the structure and to incoming seismic waves. Seismic waves may be of either natural (earthquake) or man-made (e.g. explosions) origins, and can themselves be determined by use of the displacement solutions.

Much previous work in this area has involved surface foundations on a homogeneous half-space, e.g. References 1 and 2, and has required the numerical solution of integral equations for the mixed boundary value problem. This approach has also been extended to a stratified half-space.[3] For embedded foundations, series solutions have been developed for the special case of hemispherical embedment.[4,5] Procedures applicable to arbitrary foundation geometries are reported in References 6–8.

In the following, expressions for the steady-state displacements caused by static and dynamic loads in or on a viscoelastic medium of finite depth are derived. The expressions involve no numerical integrations. In addition, no difficulties are presented by non-homogeneities; the effort required for a stratified medium is the same as that for a homogeneous medium. Although Waas[9,10] has published the displacement solutions for an isotropic material, the derivation has yet to appear in a widely available source.[11] It therefore seems useful to present the derivation in some detail. In addition, the solutions are generalized here for a transversely-isotropic material. A cylindrical coordinate system is used in the derivation, and the variation in the tangential direction is represented by a Fourier expansion. The solutions are valid for all Fourier terms. Tajimi[12] and Kausel[13,14] have derived in a different manner similar solutions for an isotropic medium. Whereas Tajimi considered only point loads, Kausel also obtained solutions for the more general case of ring loads, but only for Fourier terms 0 and 1.

Applications of the displacement solutions in the area of soil–structure interaction are illustrated. A

0098–8847/85/020173–21$02.10

Received 30 March 1984
Revised 20 August 1984

straightforward procedure is presented which extends the applicability of the solutions to the case of embedded foundations. Results are compared with previously published data.

MEDIUM

The medium consists of layers which extend horizontally to infinity. The top surface is stress-free, except for possible applied tractions. The bottom layer is bonded to a rigid base. The medium has viscoelastic transversely-isotropic material properties; i.e. the material is isotropic only in the horizontal plane. The material properties may vary with depth.

Ring loads of the form $p(\omega) = \bar{p} \cos n\theta \cdot e^{i\omega t}$ or $\bar{p} \sin n\theta \cdot e^{i\omega t}$, where ω is the circular frequency, may act in the radial, tangential or vertical directions. The medium and one possible load configuration are illustrated in Figure 1.

The displacement solutions for ring loads of the above form will be expressed in terms of solutions to an associated eigenvalue problem. The eigenvalue problem for the isotropic medium has been considered previously.[15–17] However, because the eigenvalue solution is fundamental to the displacement solution, it will be discussed in detail here.

EIGENVALUE PROBLEM

Formulation

A general displacement field in the medium can be expanded in a Fourier series (omitting, for the present, the factor $e^{i\omega t}$):

$$\mathbf{u} = \sum_{n=0}^{\infty} \left(\begin{Bmatrix} U_n^s \cos n\theta \\ W_n^s \cos n\theta \\ -V_n^s \sin n\theta \end{Bmatrix} + \begin{Bmatrix} U_n^a \sin n\theta \\ W_n^a \sin n\theta \\ V_n^a \cos n\theta \end{Bmatrix} \right) \tag{1}$$

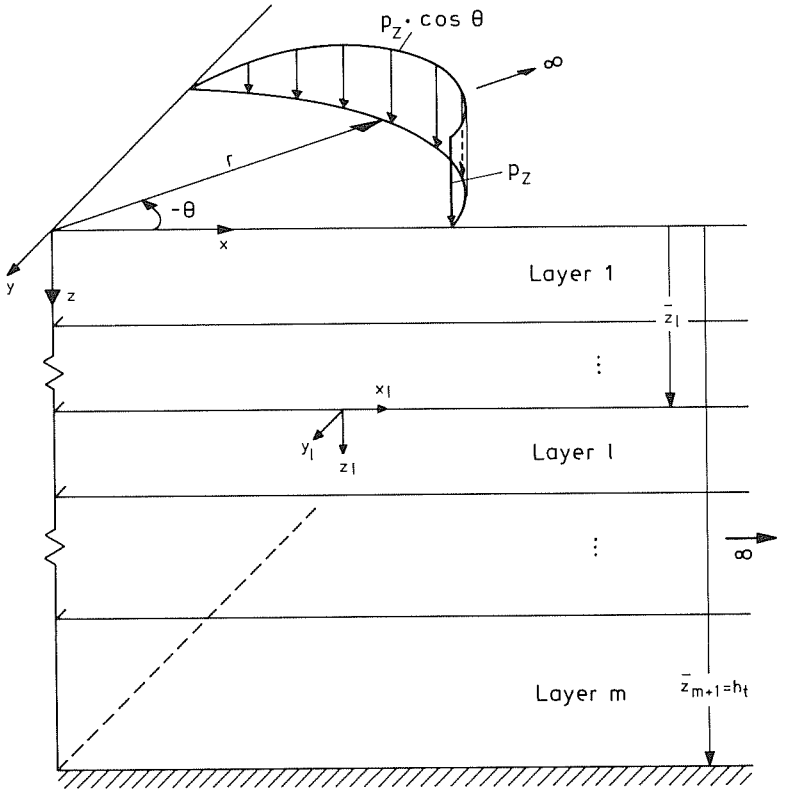

Figure 1. Horizontally infinite medium with cylindrical coordinate system and ring load

in which U_n, W_n and V_n are functions of r and z and represent the radial, vertical and tangential displacements, respectively. The superscripts 's' and 'a' refer to symmetry and antisymmetry, respectively, about $\theta = 0$. With such an expansion all relevant equations become uncoupled not only with respect to n, but also with respect to 's' and 'a'. Hence, it is necessary only to consider an arbitrary term n. Unless specifically indicated otherwise, the displacements, loads, strains and stresses will be represented here by their Fourier coefficients; for example $\mathbf{u} = \langle U, W, V \rangle^T$.

The strains and stresses consistent with the displacements $\mathbf{u}$ can be written,* respectively, as

$$\boldsymbol{\varepsilon} = \boldsymbol{\Delta}\mathbf{u} \tag{2}$$

and

$$\boldsymbol{\sigma} = \mathbf{D}\boldsymbol{\varepsilon} \tag{3}$$

$\mathbf{D}$ is the soil constitutive matrix with five independent parameters for a transversely-isotropic material. Hysteretic damping may be included by using complex-valued parameters.

The homogeneous boundary value problem for motion in the medium can be written for frequency ω as

$$\mathbf{L}_\sigma \boldsymbol{\sigma} + \rho\omega^2 \mathbf{u} = \mathbf{0} \tag{4a}$$

$$\boldsymbol{\sigma}_s = \mathbf{0} \text{ at } z = 0 \tag{4b}$$

$$\mathbf{u} = \mathbf{0} \text{ at } z = h_t \tag{4c}$$

where ρ is the mass density, and $\boldsymbol{\sigma}_s = -\langle \tau_{rz}, \sigma_{zz}, \tau_{\theta z} \rangle^T$ is the vector of stresses on the surface $z = 0$. With the use of equations (2) and (3), equation (4a) can be written in terms of displacements:

$$(\mathbf{L}_\sigma \mathbf{D} \boldsymbol{\Delta} + \rho\omega^2 \mathbf{I}_3)\mathbf{u} = \mathbf{0} \tag{5}$$

in which $\mathbf{I}_3$ is the 3×3 identity matrix.

Solutions to equation (5) may be written in the form,[17–19]

$$\mathbf{u} = (\alpha^{(1)}\mathbf{H}^{(1)} + \alpha^{(2)}\mathbf{H}^{(2)})\mathbf{f}_1 \tag{6}$$

in which $\mathbf{H}^{(1)}$ and $\mathbf{H}^{(2)}$ are matrices of Hankel functions of the first and second kind, respectively (see Appendix I). The functions are dependent on kr, where k is the yet unknown wave number. $\mathbf{f}_1$ is a vector of exponential functions dependent on k and z. $\alpha^{(1)}$ and $\alpha^{(2)}$ are participation factors.

The above analytical solution is too complex for the present purpose because the wave number k appears in the exponential functions of $\mathbf{f}_1$. It is apparent from the solution, however, that equation (5) represents a system of separable differential equations. Therefore, a solution of similar form is assumed here:

$$\mathbf{u} = \mathbf{H}\mathbf{f} \tag{7}$$

in which $\mathbf{H} = \alpha^{(1)}\mathbf{H}^{(1)} + \alpha^{(2)}\mathbf{H}^{(2)}$ and $\mathbf{f}$ is a vector of unknown functions dependent on z. If equation (7) is substituted into equation (5) and the indicated operations are carried out, the following expression results:

$$-\mathbf{H}(\mathbf{L} - \rho\omega^2 \mathbf{I}_3)\mathbf{f} = \mathbf{0} \tag{8}$$

As this must be satisfied for every value of r,

$$(\mathbf{L} - \rho\omega^2 \mathbf{I}_3)\mathbf{f} = \mathbf{0} \tag{9a}$$

Analogously, with equations (2), (3) and (7) the boundary conditions can be written as

$$\mathbf{L}_b \mathbf{f} = \mathbf{0} \text{ at } z = 0 \tag{9b}$$

$$\mathbf{f} = \mathbf{0} \text{ at } z = h_t \tag{9c}$$

From $\mathbf{L}$ and $\mathbf{L}_b$ (see Appendix I) it is apparent that the three coupled partial differential equations have been reduced to two coupled and one uncoupled ordinary differential equations which are independent of r and n.

* See Appendix I for all vectors and matrices not defined in the text.

Equations (9) represent an eigenvalue problem with k as the eigenvalue. As mentioned previously, the analytical solution is too complex for the present purpose. The finite element method will be used to obtain an approximate solution.

The domain is discretized into finite elements. (Note that the medium is discretized only in the vertical direction, and that the elements can be envisioned as infinitely long layers: see Figure 1.) The value of $\mathbf{f}$ within an element is assumed to be related to the values at the element nodes through interpolation functions. Hence, for the entire medium

$$\mathbf{f} = \mathbf{N}\mathbf{u}_e \tag{10}$$

where $\mathbf{N}$ is the matrix of interpolation functions and $\mathbf{u}_e^T = \langle \mathbf{x}^T, \mathbf{z}^T, \mathbf{y}^T \rangle$ is the vector of radial, vertical and tangential nodal 'displacements', respectively.

The FEM approximation to equations (9) can be written as

$$\left\{ \int_0^{h_t} \mathbf{N}^T \mathbf{L}_1 \mathbf{N}\, dz - \int_0^{h_t} \rho\omega^2 \mathbf{N}^T \mathbf{N}\, dz - \int_0^{h_t} \left(\frac{d}{dz} \mathbf{N}^T \right) \mathbf{L}_2 \mathbf{N}\, dz \right\} \cdot \mathbf{u}_e = \mathbf{0} \tag{11}$$

Equation (11) is most easily derived by a method of weighted residuals (Galerkin method), with a subsequent integration by parts to reduce the order of the equation. If the eigenvalue k in equation (11) is factored out and it is recognized that $\mathbf{y}$ is uncoupled from $\mathbf{x}$ and $\mathbf{z}$, then equation (11) can be written as

$$(\mathbf{A}_R k_R^2 + \mathbf{B}_R k_R + \mathbf{C}_R)\mathbf{x}_R = \mathbf{0} \tag{12a}$$

$$(\mathbf{A}_L k_L^2 + \mathbf{C}_L)\mathbf{y} = \mathbf{0} \tag{12b}$$

in which $\mathbf{x}_R^T = \langle \mathbf{x}^T, \mathbf{z}^T \rangle$. Equations (12a) and (12b) are the algebraic eigenvalue equations for generalized Rayleigh and Love waves, respectively, with the wave numbers k_R and k_L as the eigenvalues. Equations (11) and (12) are general, as no assumptions have been made concerning the interpolation functions (except that $\mathbf{f}$ is $C^{(0)}$ continuous) or the variation with depth of the material properties. If such assumptions are made, the integrals in equation (11) [or the integrals implicit in equations (12)] can be evaluated. It will be assumed here that $\mathbf{f}$ varies linearly within an element. Furthermore, it will be assumed that the material properties are constant within an element, but that they may vary from element to element. The matrices in equations (12) for this case are given in Appendix I in terms of the corresponding element matrices. The global matrices are formed from the element matrices using standard finite element assembly procedures.

Solution

Waas[16] has discussed the solutions to the above equations in detail. Only a brief discussion is necessary here. Equations (12a) and (12b) represent $2m$ and m equations, respectively, where m is the total number of layers. There are, however, $6m$ solutions. (If k is one eigenvalue, then $-k$ is also an eigenvalue.) When the eigensolutions are combined with the two Hankel functions, $12m$ wave patterns result. However, as there are only $6m$ linearly independent patterns it is assumed here that only those $3m$ eigenvalues with negative imaginary parts are used. In case of real eigenvalues the direction of energy flow has to be observed in choosing the eigenvalues.[16]

Certain orthogonality relations of the eigenvectors will be employed to solve for the displacements caused by ring loads. The orthogonality relations for Love waves, with the indicated normalization of the eigenvectors, are easily shown to be

$$\mathbf{Y}^T \mathbf{A}_L \mathbf{Y} = \mathbf{K}_L^{-2} \tag{13a}$$

$$\mathbf{Y}^T \mathbf{C}_L \mathbf{Y} = -\mathbf{I} \tag{13b}$$

where $\mathbf{Y}$ is the matrix of the $\mathbf{y}$ eigenvectors and $\mathbf{K}_L$ is the diagonal matrix of Love wave numbers.

The orthogonality relations for Rayleigh waves can be written for solutions i and j as[16]

$$k_{Rj} \mathbf{x}_{Rj}^T \mathbf{A}_R \mathbf{x}_{Ri} k_{Ri} - \mathbf{x}_{Rj}^T \mathbf{C}_R \mathbf{x}_{Ri} = \begin{cases} 0 & i \neq j \\ 2 & i = j \end{cases} \tag{14}$$

With the property that k_{Ri}, $\mathbf{x}_{Ri}^{T} = \langle \mathbf{x}_i^{T}, \mathbf{z}_i^{T} \rangle$ and $-k_{Ri}$, $\langle -\mathbf{x}_i^{T}, \mathbf{z}_i^{T} \rangle$ are both solutions, the orthogonality relations can be written for all eigenvectors as

$$\mathbf{K}_R \mathbf{Z}^T \mathbf{A}_z \mathbf{Z} \mathbf{K}_R - \mathbf{X}^T \mathbf{C}_x \mathbf{X} = \mathbf{I} \tag{15a}$$

$$\mathbf{K}_R \mathbf{X}^T \mathbf{A}_x \mathbf{X} \mathbf{K}_R - \mathbf{Z}^T \mathbf{C}_z \mathbf{Z} = \mathbf{I} \tag{15b}$$

in which $\mathbf{K}_R$ is the diagonal matrix of Rayleigh wave numbers, and $\mathbf{X}$ and $\mathbf{Z}$ are the $m \times 2m$ matrices with columns i equal to $\mathbf{x}_i$ and $\mathbf{z}_i$, respectively. For further orthogonality relations see Reference 14.

DISPLACEMENTS CAUSED BY RING LOADS

The displacements in the medium caused by dynamic ring loads applied at the layer boundaries along the interface $r = r_0$ are now sought. For this purpose it is necessary to consider two regions: region I is defined by $r \leqslant r_0$, and region II is defined by $r \geqslant r_0$ (Figure 2). The displacements will be expanded in terms of the solutions of the homogeneous problem; i.e. in the form of equation (7):

$$\mathbf{u}_b = \sum_{j=1}^{2m} (\alpha_{Rj}^{(1)} \mathbf{H}_{Rj}^{(1)} + \alpha_{Rj}^{(2)} \mathbf{H}_{Rj}^{(2)}) \mathbf{x}_{Rj} + \sum_{j=1}^{m} (\alpha_{Lj}^{(1)} \mathbf{H}_{Lj}^{(1)} + \alpha_{Lj}^{(2)} \mathbf{H}_{Lj}^{(2)}) \mathbf{y}_j \tag{16}$$

where $\mathbf{u}_b$ are the displacements along the layer boundaries. The matrices are defined in Appendix I.

For the $3m$ eigenvalues which were chosen, the Hankel functions of the first kind represent waves which propagate from infinity towards the origin, whereas the reverse is true for Hankel functions of the second kind. In region II, waves of the first type are a physical impossibility; hence $\alpha_j^{(1)} \equiv 0$. The layer displacements in region II are therefore

$$\mathbf{u}_b^{II} = \sum_{j=1}^{2m} \mathbf{H}_{Rj}^{(2)} \mathbf{x}_{Rj} \alpha_{Rj}^{(2)} + \sum_{j=1}^{m} \mathbf{H}_{Lj}^{(2)} \mathbf{y}_j \alpha_{Lj}^{(2)} \tag{17a}$$

Henceforth, the superscript '(2)' will be dropped for convenience.

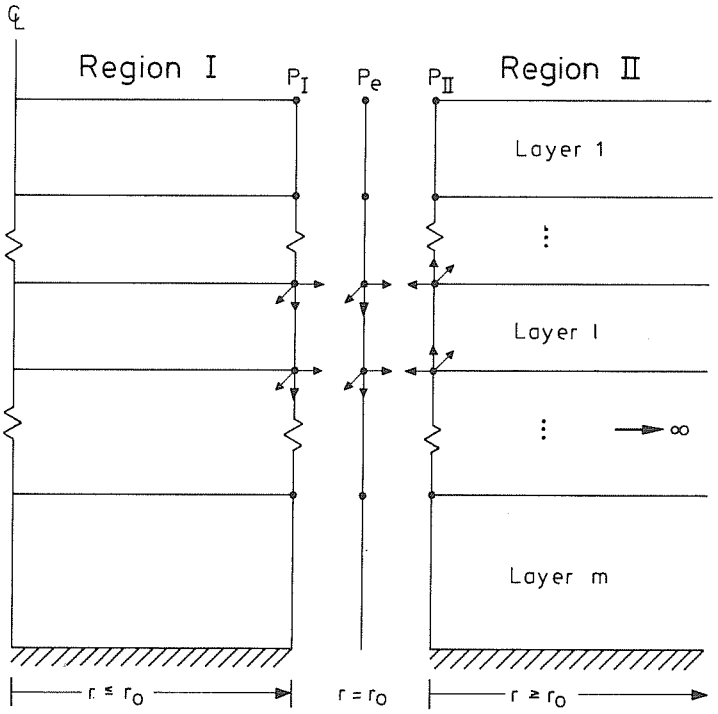

Figure 2. Subdivision of medium into region I and region II, with $\mathbf{p}_e$, $\mathbf{p}_I$, and $\mathbf{p}_{II}$ at layer l

In region I, both waves propagating to and from the origin are possible. However, from continuity requirements at the origin it follows that $\alpha_j^{(1)} \equiv \alpha_j^{(2)}$. With the identity $H_n^{(1)}(kr) + H_n^{(2)}(kr) \equiv J_n(kr)$, the displacements are

$$\mathbf{u}_b^{\mathrm{I}} = \sum_{j=1}^{2m} \mathbf{J}_{\mathrm{R}j} \mathbf{x}_{\mathrm{R}j} \beta_{\mathrm{R}j} + \sum_{j=1}^{m} \mathbf{J}_{\mathrm{L}j} \mathbf{y}_j \beta_{\mathrm{L}j} \tag{17b}$$

where β has been used for the participation factors in region I. $\mathbf{J}_{\mathrm{R}j}$ and $\mathbf{J}_{\mathrm{L}j}$ are similar to $\mathbf{H}_{\mathrm{R}j}$ and $\mathbf{H}_{\mathrm{L}j}$, but with the Hankel functions replaced by Bessel functions.

The $4m$ factors $\alpha_{\mathrm{R}j}$, $\beta_{\mathrm{R}j}$ and $2m$ factors $\alpha_{\mathrm{L}j}$, $\beta_{\mathrm{L}j}$ are as yet unknown. The $6m$ equations necessary to determine the participation factors are provided by displacement continuity and force equilibrium along the interface $r = r_0$. Displacement continuity gives

$$\mathbf{u}_b^{\mathrm{I}}(r = r_0) = \mathbf{u}_b^{\mathrm{II}}(r = r_0) \tag{18a}$$

or, subtracting equation (17b) from equation (17a):

$$\sum_{j=1}^{2m} (\mathbf{H}_{\mathrm{R}j} \alpha_{\mathrm{R}j} - \mathbf{J}_{\mathrm{R}j} \beta_{\mathrm{R}j}) \mathbf{x}_{\mathrm{R}j} + \sum_{j=1}^{m} (\mathbf{H}_{\mathrm{L}j} \alpha_{\mathrm{L}j} - \mathbf{J}_{\mathrm{L}j} \beta_{\mathrm{L}j}) \mathbf{y}_j = \mathbf{0} \tag{18b}$$

in which the Hankel and Bessel functions are evaluated at $r = r_0$.

The following substitution of variables significantly simplifies equation (18b):

$$\alpha_{\mathrm{R}j} = J_n a_j + J_n' c_j \tag{19a}$$

$$\beta_{\mathrm{R}j} = H_n^{(2)} a_j + H_n^{(2)\prime} c_j \tag{19b}$$

$$\alpha_{\mathrm{L}j} = J_n b_j + J_n' d_j \tag{19c}$$

$$\beta_{\mathrm{L}j} = H_n^{(2)} b_j + H_n^{(2)\prime} d_j \tag{19d}$$

where the functions are evaluated at $k_{\mathrm{R}j} \cdot r_0$ for $\alpha_{\mathrm{R}j}$, $\beta_{\mathrm{R}j}$ and at $k_{\mathrm{L}j} \cdot r_0$ for $\alpha_{\mathrm{L}j}$, $\beta_{\mathrm{L}j}$, and $(\,)' \equiv \mathrm{d}(\,)/\mathrm{d}r$. With the relation $H_n^{(2)} J_n' - H_n^{(2)\prime} J_n = 2\mathrm{i}/\pi r_0$, equation (18b) then becomes

$$\sum_{j=1}^{2m} -\mathbf{x}_j a_j + \frac{n}{r} \sum_{j=1}^{m} \mathbf{y}_j d_j = \mathbf{0} \quad \text{or} \quad -\mathbf{X}\mathbf{a} + \frac{n}{r} \mathbf{Y}\mathbf{d} = \mathbf{0} \tag{20a}$$

$$\sum_{j=1}^{2m} k_{\mathrm{R}j} c_j \mathbf{z}_j = \mathbf{0} \quad \text{or} \quad \mathbf{Z}\mathbf{K}_{\mathrm{R}}\mathbf{c} = \mathbf{0} \tag{20b}$$

$$\frac{n}{r} \sum_{j=1}^{2m} c_j \mathbf{x}_j + \sum_{j=1}^{m} -b_j \mathbf{y}_j = \mathbf{0} \quad \text{or} \quad \frac{n}{r} \mathbf{X}\mathbf{c} - \mathbf{Y}\mathbf{b} = \mathbf{0} \tag{20c}$$

The final $3m$ constraint equations necessary to determine the displacements are obtained from the requirement of force equilibrium along the interface at $r = r_0$:

$$\mathbf{p}_e = \mathbf{p}_{\mathrm{I}} - \mathbf{p}_{\mathrm{II}} \tag{21}$$

The 'nodal' forces $\mathbf{p}_e{}^{\mathrm{T}} = \langle \mathbf{p}_r^{\mathrm{T}}, \mathbf{p}_z^{\mathrm{T}}, \mathbf{p}_\theta^{\mathrm{T}} \rangle$ are the externally applied ring loads of the form $p\mathrm{e}^{\mathrm{i}\omega t}$ and with either a sine or cosine expansion in the θ direction. The nodal forces $\mathbf{p}_{\mathrm{II}}$ and $\mathbf{p}_{\mathrm{I}}$ are the consistent nodal loads that are in equilibrium, in an energy sense, with the surface stress distribution along the interface $r = r_0$.

The relation between the stresses and the nodal forces can be obtained by the principle of virtual displacements. For layer l this can be written as

$$\mathbf{p}^l = \int_{h_l} \mathbf{N}_l{}^{\mathrm{T}} \mathbf{T}^{\mathrm{T}} \boldsymbol{\sigma} \, \mathrm{d}z = \int_{h_l} \mathbf{N}_l{}^{\mathrm{T}} \mathbf{T}^{\mathrm{T}} \mathbf{D} \boldsymbol{\Delta} \mathbf{u} \, \mathrm{d}z \tag{22}$$

$\mathbf{T}$ is a transformation matrix such that $\mathbf{T}^{\mathrm{T}}\boldsymbol{\sigma}$ is the vector of surface stresses $\langle \sigma_{rr}, \tau_{rz}, \tau_{r\theta} \rangle^{\mathrm{T}}$. The displacements in equation (22) can be expressed in terms of the layer boundary displacements with equations (17), and the

interpolation matrix $\mathbf{N}_l$. If the integrations along the two surfaces are performed for all layers, and the resulting expressions are simplified by the use of equations (19) and (20), the following equations are obtained:

$$\frac{\pi r_0}{2\mathrm{i}}\mathbf{p}_r = \mathbf{A}_x \mathbf{X} \mathbf{K}_\mathrm{R}^2 \mathbf{c} \tag{23a}$$

$$\frac{\pi r_0}{2\mathrm{i}}\mathbf{p}_z = \mathbf{A}_z \mathbf{Z} \mathbf{K}_\mathrm{R} \mathbf{a} \tag{23b}$$

$$\frac{\pi r_0}{2\mathrm{i}}\mathbf{p}_\theta = \mathbf{A}_\mathrm{L} \mathbf{Y} \mathbf{K}_\mathrm{L}^2 \mathbf{d} \tag{23c}$$

Equations (20) and (23) represent $6m$ equations in $6m$ unknowns. An explicit solution for the unknowns is possible with use of the orthogonality conditions. For example, the solution for $\mathbf{d}$ is apparent from equations (23c) and (13a). The following relations result:

$$\mathbf{a} = -\mathrm{i}\frac{\pi r_0}{2}\left(\mathbf{K}_\mathrm{R}\mathbf{Z}^\mathrm{T}\mathbf{p}_z + \frac{n}{r_0}\mathbf{X}^\mathrm{T}\mathbf{p}_\theta\right) \tag{24a}$$

$$\mathbf{b} = -\mathrm{i}\frac{\pi}{2} n \mathbf{Y}^\mathrm{T}\mathbf{p}_r \tag{24b}$$

$$\mathbf{c} = -\mathrm{i}\frac{\pi r_0}{2}\mathbf{X}^\mathrm{T}\mathbf{p}_r \tag{24c}$$

$$\mathbf{d} = -\mathrm{i}\frac{\pi r_0}{2}\mathbf{Y}^\mathrm{T}\mathbf{p}_\theta \tag{24d}$$

The displacements along the layer boundaries for ring loads at $r = r_0$ and for any Fourier term n is thus given by equations (17), (19) and (24). For ring loads at $r = r_0$, the radial, vertical and tangential displacements of the layer boundaries at $r = R \geqslant r_0$ are:

$$\mathbf{u} = -\mathrm{i}\frac{\pi}{2}\left(\sum_{j=1}^{2m} H'_j \mathbf{x}_j \alpha_{\mathrm{R}j} + \frac{n}{R}\sum_{j=1}^{m} \bar{H}_j \mathbf{y}_j \alpha_{\mathrm{L}j}\right)\begin{pmatrix}\cos n\theta \\ \sin n\theta\end{pmatrix}\cdot \mathrm{e}^{\mathrm{i}\omega t} \tag{25a}$$

$$\mathbf{w} = -\mathrm{i}\frac{\pi}{2}\left(\sum_{j=1}^{2m} k_{\mathrm{R}j} H_j \mathbf{z}_j \alpha_{\mathrm{R}j}\right)\begin{pmatrix}\cos n\theta \\ \sin n\theta\end{pmatrix}\cdot \mathrm{e}^{\mathrm{i}\omega t} \tag{25b}$$

$$\mathbf{v} = -\mathrm{i}\frac{\pi}{2}\left(\frac{n}{R}\sum_{j=1}^{2m} H_j \mathbf{x}_j \alpha_{\mathrm{R}j} + \sum_{j=1}^{m} \bar{H}'_j \mathbf{y}_j \alpha_{\mathrm{L}j}\right)\begin{pmatrix}-\sin n\theta \\ \cos n\theta\end{pmatrix}\cdot \mathrm{e}^{\mathrm{i}\omega t} \tag{25c}$$

where $H_j = H_n^{(2)}(k_{\mathrm{R}j}R)$, $\bar{H}_j = H_n^{(2)}(k_{\mathrm{L}j}R)$, and the common term $-\mathrm{i}\pi/2$ has been factored out of the participation factors.

The participation factors for various load conditions are as follows:

Radial ring load layer l,

$$\begin{aligned} p &= p_r\begin{pmatrix}\cos n\theta \\ \sin n\theta\end{pmatrix} \\ \alpha_{\mathrm{R}j} &= r_0 J'_j X_{lj} p_r \\ \alpha_{\mathrm{L}j} &= n\bar{J}_j Y_{lj} p_r \end{aligned} \tag{26a}$$

Vertical ring load at layer l,

$$\begin{aligned} p &= p_z\begin{pmatrix}\cos n\theta \\ \sin n\theta\end{pmatrix} \\ \alpha_{\mathrm{R}j} &= r_0 J_j k_{\mathrm{R}j} Z_{lj} p_z \\ \alpha_{\mathrm{L}j} &= 0 \end{aligned} \tag{26b}$$

Tangential ring load at layer l,

$$p = p_\theta \begin{pmatrix} -\sin n\theta \\ \cos n\theta \end{pmatrix}$$

$$\alpha_{Rj} = nJ_j X_{lj} p_\theta \qquad (26c)$$

$$\alpha_{Lj} = r_0 \bar{J}'_j Y_{lj} p_\theta$$

where $J_j = J_n(k_{Rj} r_0)$, $\bar{J}_j = J_n(k_{Lj} r_0)$, and X_{lj} is the (l, j) element of $\mathbf{X}$, etc. If $R < r_0$, then Bessel functions instead of Hankel functions must be used in equations (25), and Hankel instead of Bessel functions must be used in equations (26). (The Hankel functions must always be evaluated at the larger of R and r_0.)

For an isotropic medium the above solutions can be shown to be equivalent to those given in Reference 13.

The solutions for ring loads can be used to determine the displacements caused by point, line and disk loads. These solutions are given in Appendix II.

APPLICATIONS

Soil stiffness matrix

One application of the above solutions is in soil–structure interaction analyses of axisymmetric structures. With the displacement solutions, a frequency-dependent flexibility matrix which relates forces and displacements at a number of rings in the soil can be easily constructed. The dynamic stiffness matrix, $\mathbf{K}_m(\omega)$, is obtained by inversion. $\mathbf{K}_m(\omega)$ may be added to the structure dynamic stiffness matrix at the corresponding foundation degrees-of-freedom to obtain the global stiffness matrix, which can be used for dynamic analyses in the frequency domain. Frequently only the Fourier terms $n = 0$ (vertical and torsional motion) and $n = 1$ (horizontal and rocking motion) are necessary.

In the theory presented the soil medium is discretized in the vertical direction by several thin layers, or sublayers. It is also discretized in the horizontal direction, insofar as the soil and foundation are connected at a finite number of rings. Directly underneath the foundation, the vertical discretization must be able to represent the local soil–foundation interaction effects, and relatively thin layer thicknesses are required. At a larger depth, in order that elastic waves are adequately represented by the assumed displacement functions, the layer thickness is limited to approximately 1/6 the length of a shear wave. A study has indicated that for an isotropic medium (Poisson's ratio $\nu = 1/3$), the best horizontal discretization is obtained when the nodal ring spacing equals the layer thickness directly underneath the foundation.

For rigid foundations, frequency-dependent 'foundation' stiffnesses (soil springs) can be easily computed from the soil flexibility or stiffness matrices. In this section, stiffnesses of rigid surface and embedded foundations are compared with previously published results in order to verify the validity of the displacement solutions. In addition, results for a rigid surface foundation on a soil with a linearly increasing shear modulus are presented.

Surface foundations

The frequency-dependent stiffnesses of rigid circular surface foundations on a homogeneous viscoelastic half-space have been computed previously.[3] In addition, approximate formulae for the static stiffnesses of rigid foundations on a homogeneous, elastic layer with a rigid base have been developed based on finite element parameter studies.[20,21]

With the displacement solutions from above, the dynamic stiffnesses of a rigid circular foundation on a deep soil layer ($h_l/a = 10$, a = foundation radius) have been computed. The shear modulus was assumed to increase linearly with depth:

$$G(z) = G_0\left(1 + \gamma \cdot \frac{z}{a}\right)$$

Three cases, $\gamma = 0$, 1 and 2, were studied using $\nu = 1/3$ and a material damping ratio $D = 0{\cdot}05$. The soil layer was modelled with 40 sublayers of varying thicknesses: $8 \times 0{\cdot}1a$, $4 \times 0{\cdot}15a$, $4 \times 0{\cdot}2a$, $4 \times 0{\cdot}25a$ and $20 \times 0{\cdot}34a$. The foundation and soil were coupled at 10 equally spaced nodal rings.

The dynamic stiffnesses can be written in terms of static stiffnesses K_{ii}^s and frequency-dependent non-dimensional stiffness coefficients, k_{ii} and c_{ii} (or $\tilde{k}_{ii}$ and $\tilde{c}_{ii}$):

$$K_{ii} = K_{ii}^s \cdot (k_{ii} + ia_0 c_{ii})$$

or

$$K_{ii} = K_{ii}^s \cdot (1 + i2D) \cdot (\tilde{k}_{ii} + ia_0 \tilde{c}_{ii})$$

where $a_0 = \omega \cdot a/c_s$ is the non-dimensional frequency and $c_s = \sqrt{(G_0/\rho)}$ is the shear wave velocity. The static stiffnesses computed here, together with the values for a half-space and the values from the above-mentioned formulae for an elastic layer, are given in Table I. The results for the homogeneous layer ($\gamma = 0$) agree well with the other results. The results for $\gamma = 1$ and 2 indicate that the stiffnesses increase significantly for a variable shear modulus. The largest increase is in the vertical stiffness.

The non-dimensional stiffness coefficients are plotted in Figure 3. The available values for the homogeneous half-space[3] are also plotted. (The results for torsion were not given in Reference 3.) Agreement between the layer ($h_t/a = 10$) and the half-space is good. However, the horizontal and vertical stiffness coefficients for the layer show some waviness, which is caused by wave reflections at the rigid base. A linear variation of the shear modulus affects the coefficients k_{ii} only slightly. However, the coefficients c_{ii} and thus the equivalent viscous damping ratio $D = 0{\cdot}5a_0 c_{ii}/k_{ii}$ are significantly affected by the variation of the shear modulus with depth. (Note that a_0 is based on the modulus at the soil surface.)

The static stiffnesses of a rigid foundation on a transversely-isotropic elastic soil layer were computed and compared with the results of Kirkner[22] for a half-space. A deep layer ($h_t/a = 20$) was discretized into 34 sublayers: $9 \times 0{\cdot}1a$, $4 \times 0{\cdot}15a$, $4 \times 0{\cdot}225a$, $4 \times 0{\cdot}375a$, $4 \times 0{\cdot}65a$ and $9 \times 1{\cdot}5a$. The material properties were: $D_{rr} = 4G_{rz}$, $D_{rz} = 0{\cdot}732G_{rz}$, $D_{zz} = 2G_{rz}$ and $G_{r\theta} = 2{\cdot}5G_{rz}$. The foundation and soil were coupled at 10 equally spaced nodal rings at which the relaxed boundary conditions of Kirkner were imposed. The results are compared in Table II and can be seen to be in good agreement. A mesh refinement resulted in a change in stiffness of approximately 1 per cent in each of the three cases.

Embedded foundations

The complex frequency-dependent stiffness matrix $\mathbf{K}_m(\omega)$ relates forces and displacements at nodal rings in and on a horizontally layered medium, Figure 4(a). If there is an excavation, $\mathbf{K}_m(\omega)$ includes the inertia, damping and elastic forces of the excavated soil. Hence, the stiffness must be modified to account for the excavation.

If the excavated soil is modelled with solid finite elements with the appropriate Fourier expansion in the circumferential direction, Figure 4(b), the excavation mass matrix $\mathbf{M}$ and complex stiffness matrix $\mathbf{K}$ can be easily computed. The following relationship then may be written for the excavation:

$$[\mathbf{K} - \omega^2\mathbf{M}] = \begin{bmatrix} \mathbf{K}_{ii} - \omega^2\mathbf{M}_{ii} & \mathbf{K}_{ib} - \omega^2\mathbf{M}_{ib} \\ \mathbf{K}_{bi} - \omega^2\mathbf{M}_{bi} & \mathbf{K}_{bb} - \omega^2\mathbf{M}_{bb} \end{bmatrix} \begin{Bmatrix} \mathbf{u}_i \\ \mathbf{u}_b \end{Bmatrix} = \begin{Bmatrix} \mathbf{0} \\ \mathbf{f}_b \end{Bmatrix} \tag{27}$$

in which $\mathbf{u}$ is the displacement vector, $\mathbf{f}_b$ is the vector of unknown boundary interaction forces between the soil and the excavation, and the subscripts 'i' and 'b' refer to the internal and boundary degrees of freedom,

Table I. Static stiffnesses of a rigid circular foundation on the surface of a half-space and a layer for $\nu = 1/3$

Stiffness component	Half-space[3]	Layer, $h_t/a = 10$			
		Approximation[20,21]	Present method		
		$\gamma = 0$	$\gamma = 0$	$\gamma = 1$	$\gamma = 2$
Horizontal $K_{HH}^s/(G_0 \cdot a)$	4·80	5·04	5·09	7.62	9·35
Rocking $K_{RR}^s/(G_0 \cdot a^3)$	4·00	4·07	4·02	5·61	6·82
Vertical $K_{VV}^s/(G_0 \cdot a)$	6·00	6·77	6·60	12·83	17·03
Torsion $K_{TT}^s/(G_0 \cdot a^3)$	5·33	5·33	5·33	6·40	7·28

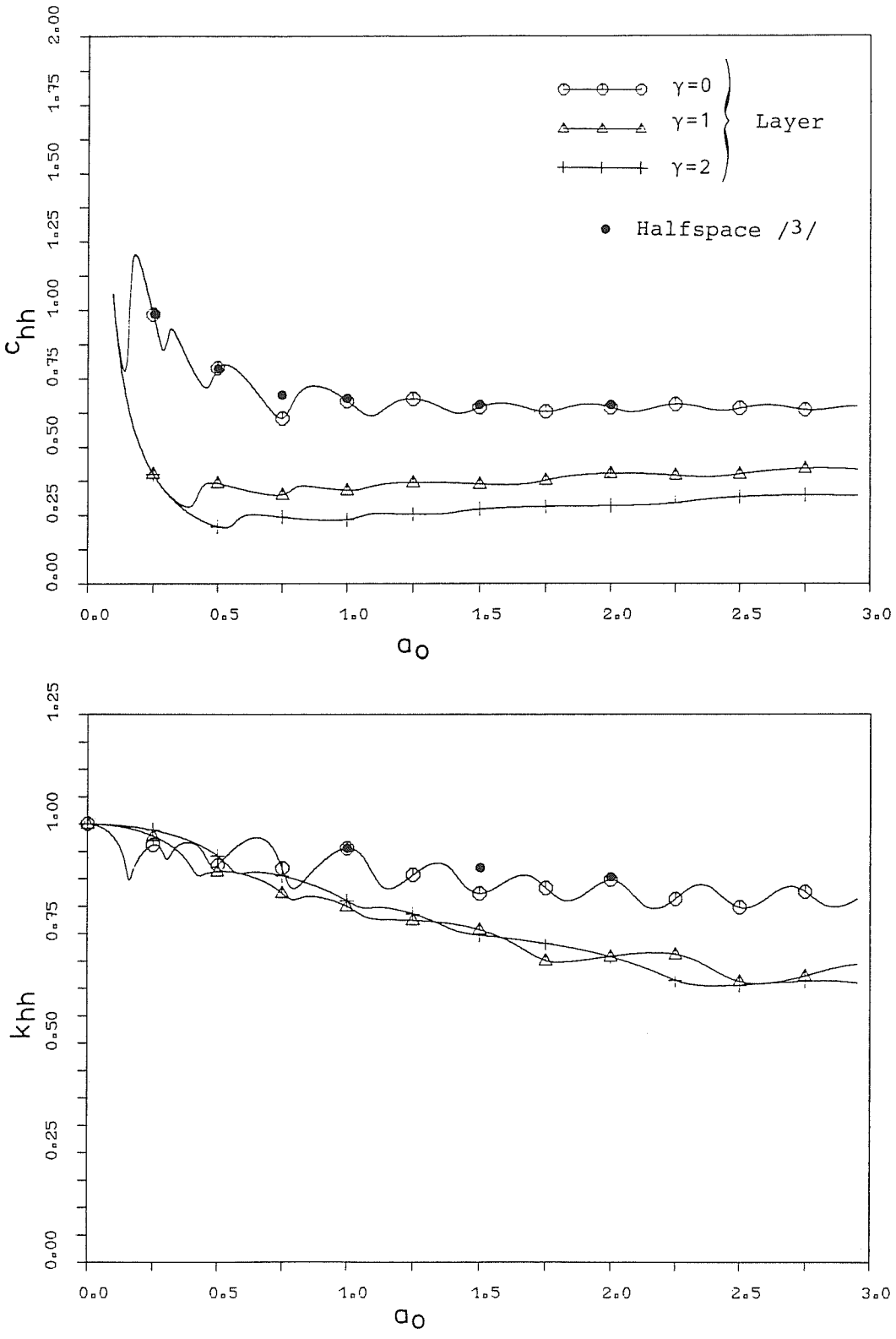

Figure 3(a). Non-dimensional stiffness coefficients k_{ii}, c_{ii} vs. frequency a_0; $\nu = 1/3$, $D = 0{\cdot}05$, layer $h_l/a = 10$. Horizontal stiffness

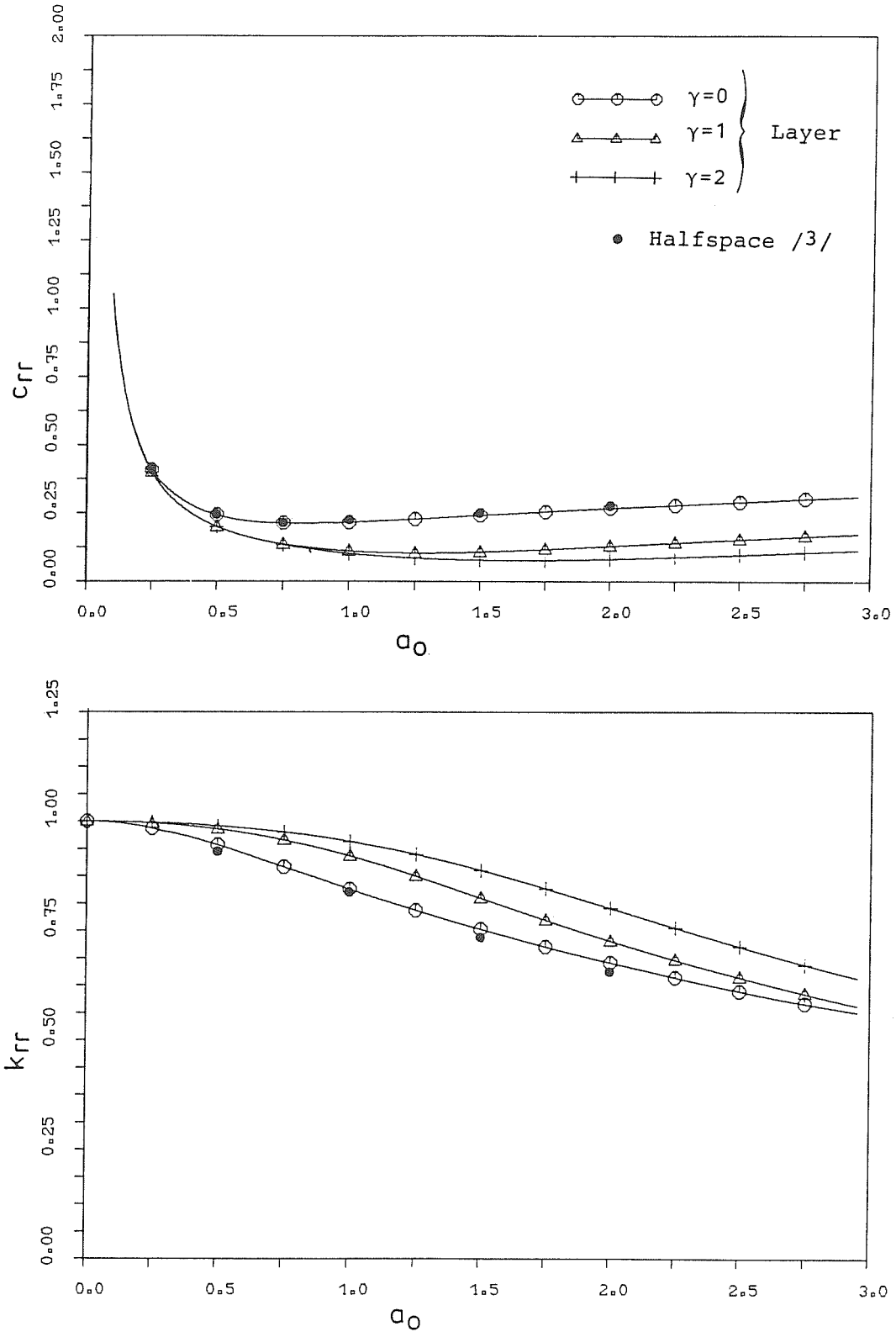

Figure 3(b). Non-dimensional stiffness coefficients k_{ii}, c_{ii} vs. frequency a_0; $\nu = 1/3$, $D = 0{\cdot}05$, layer $h_l/a = 10$. Rocking stiffness

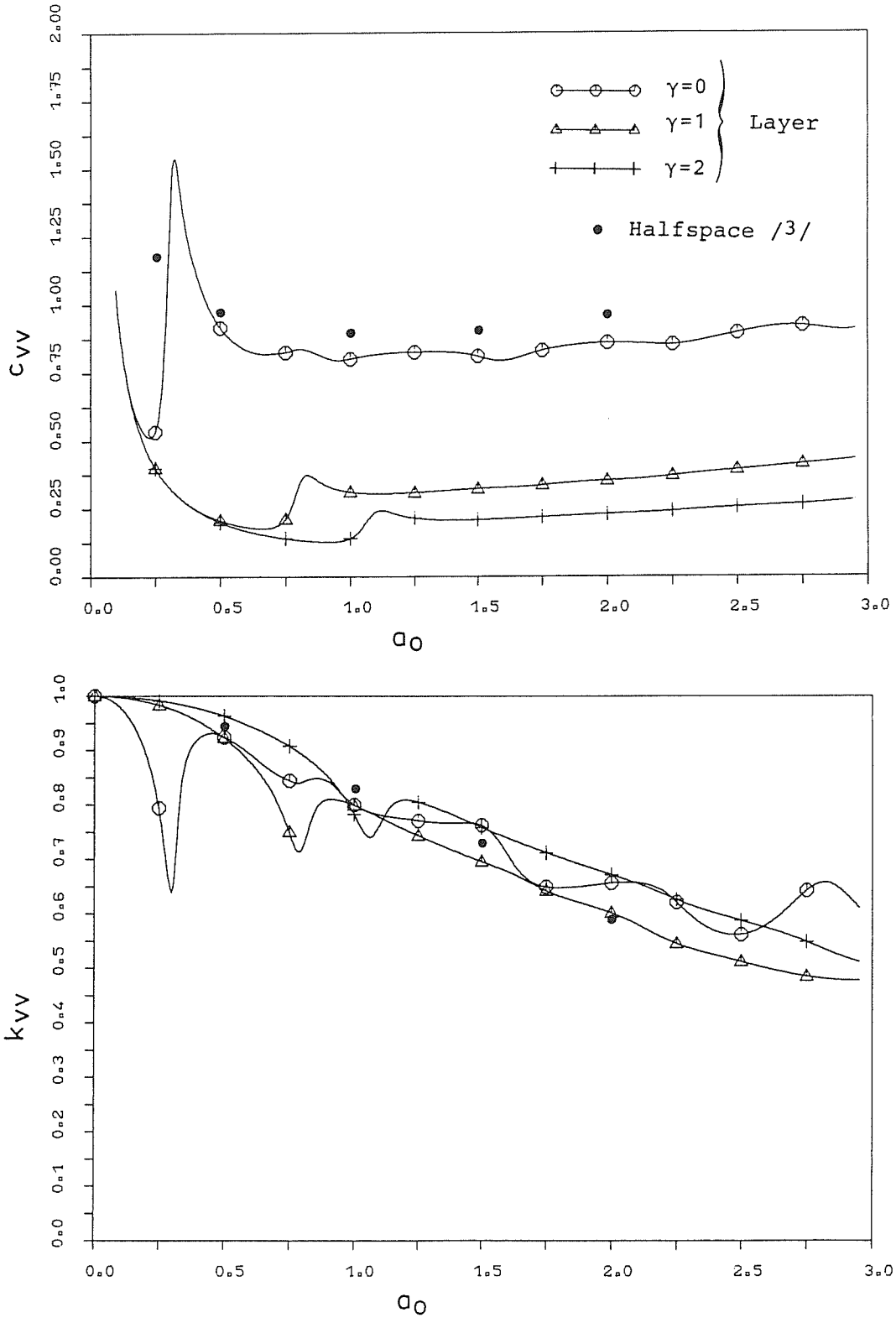

Figure 3(c). Non-dimensional stiffness coefficients k_{ii}, c_{ii} vs. frequency a_0; $\nu = 1/3$, $D = 0{\cdot}05$, layer $h_l/a = 10$. Vertical stiffness

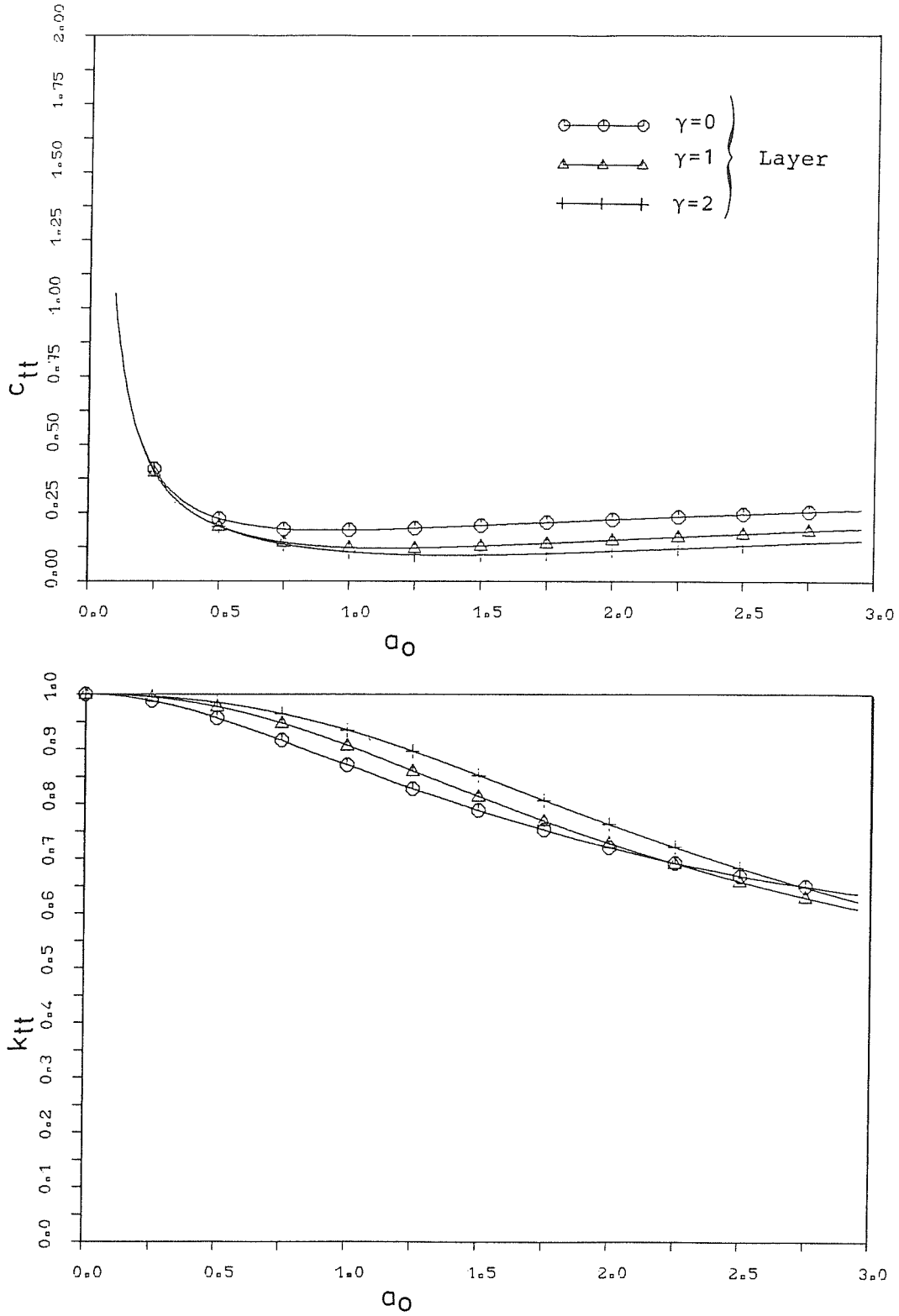

Figure 3(d). Non-dimensional stiffness coefficients k_{ii}, c_{ii} vs. frequency a_0; $\nu = 1/3$, $D = 0{\cdot}05$, layer $h_1/a = 10$. Torsional stiffness

Table II. Static stiffnesses for rigid circular foundation on transversely-isotropic elastic soil

	Horizontal $K^s_{HH}/(G_{rz} \cdot a)$	Rocking $K^s_{RR}/(G_{rz} \cdot a^3)$	Vertical $K^s_{VV}/(G_{rz} \cdot a)$
Layer $h_t/a = 20$	6·49	2·93	4·50
Half-space[22]	6·25	2·92	4·37

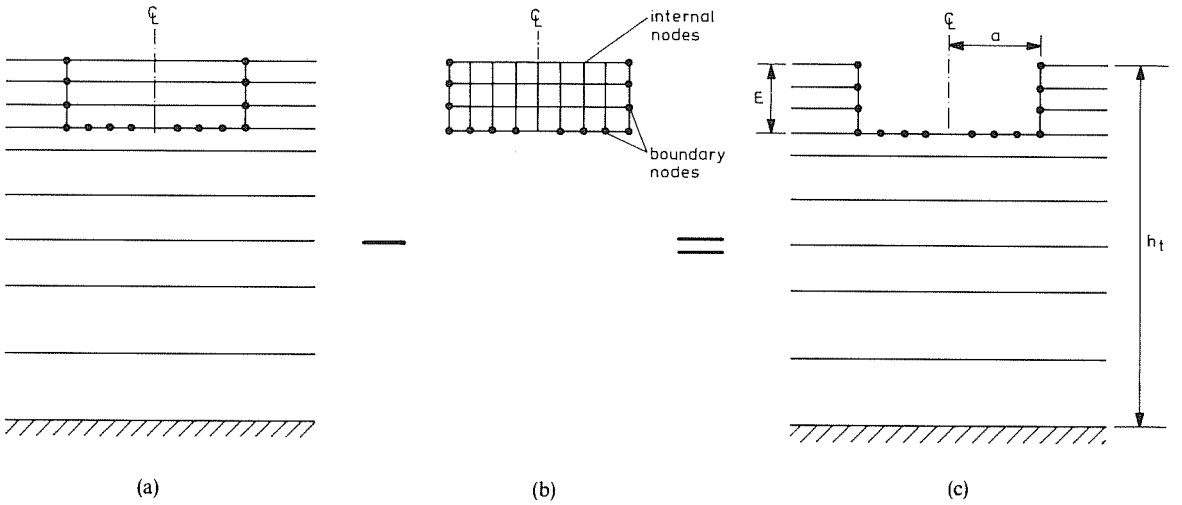

Figure 4. Stiffness modification for an excavation: (a) horizontally layered medium; (b) excavation modelled with finite elements; (c) medium with excavation

respectively. The internal degrees-of-freedom can be condensed out of equation (27), resulting in the boundary stiffness matrix $\mathbf{K}_b(\omega)$. The dynamic stiffness matrix $\mathbf{K}_g(\omega)$ of the soil with an excavation then can be obtained as

$$\mathbf{K}_g(\omega) = \mathbf{K}_m(\omega) - \mathbf{K}_b(\omega)$$

The procedure is illustrated in Figure 4. For purely elastic media, numerical difficulties arise when ω is sufficiently close to the natural frequencies of the excavation.[8]

The above procedure has been used to compute the horizontal and rocking stiffnesses of an embedded rigid foundation for the case $h_t/a = 3$, $E/a = 1$, $\nu = 1/3$ and $D = 0{\cdot}05$. For the homogeneous soil layer, 24 sublayers of equal height were used. The excavation was modelled with 64 solid elements of equal size. The static stiffnesses for this case are $K^0_{HH}/(G_0 \cdot a) = 13{\cdot}8$ and $K^0_{RR}/(G_0 \cdot a^3) = 16{\cdot}3$, which agree well with the corresponding values of 13·2 and 15·6 obtained from the approximate formulae developed in Reference 21. The dynamic stiffness coefficients are presented in Figure 5, together with the results of Elsabee and Morray.[21] The latter used a transmitting boundary for the soil away from the foundation, and finite elements for the soil under the foundation. The good agreement between the results illustrates the effectiveness of the above-described modification for excavations.

CONCLUSIONS

Displacement solutions for loads in a layered viscoelastic medium have been derived. The solutions provide a versatile method of computing soil stiffness matrices for use in soil–structure interaction problems. Stratification of the medium causes neither difficulty nor additional effort. With a straightforward numerical

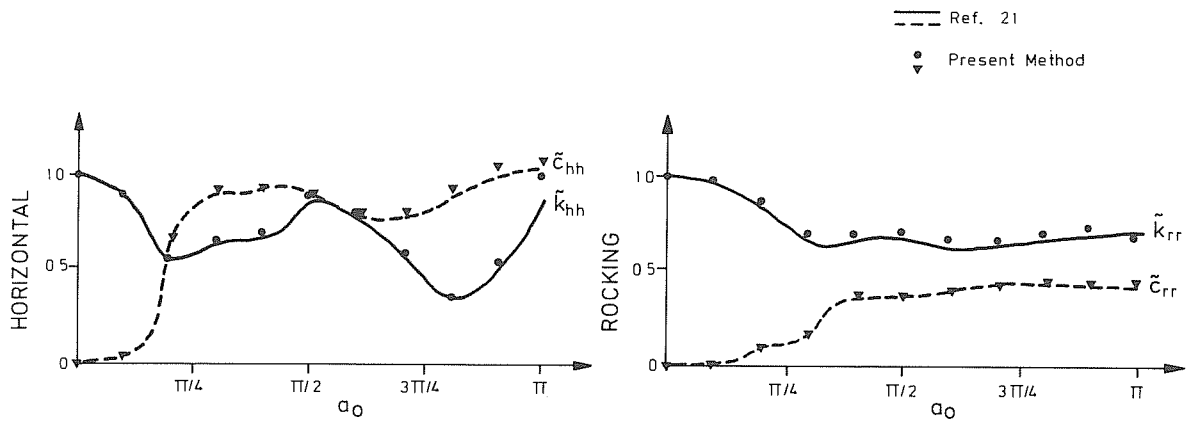

Figure 5. Non-dimensional stiffness coefficients $\tilde{k}_{ii}, \tilde{c}_{ii}$ vs. frequency a_0 for an embedded foundation; $\nu = 1/3, D = 0{\cdot}05, h_t/a = 3, E/a = 1$

modification procedure, embedded foundations of arbitrary geometry can be modelled with good accuracy. The assumption of a rigid base underneath the medium means that the solutions are most applicable to soil layers underlain by a much stiffer soil or bedrock. However, the solutions also can be used for viscoelastic half-spaces if the soil is modelled to a large enough depth.

Agreement between the present results and previously published data is good. The impedance functions for a rigid foundation on a soil with a shear modulus which increases linearly with depth have been presented. The results have shown that the variation of the modulus significantly affects the damping coefficient of the foundation.

The displacement solutions presented herein have a wide range of applicability. An application in soil–structure interaction with axisymmetric rigid foundations has been illustrated here. Flexibility of the foundation also can be considered.[23] The solutions for point loads have been applied to non-axisymmetric foundations and structure–soil–structure interaction problems,[24] and to pile foundations.[10] The method also has been used to solve wave propagation and kinematic interaction problems.[25, 26]

APPENDIX I—VECTORS AND MATRICES

$$\boldsymbol{\varepsilon} = \langle \varepsilon_{rr}, \varepsilon_{\theta\theta}, \varepsilon_{zz}, \gamma_{rz}, \gamma_{r\theta}, \gamma_{\theta z} \rangle^{\mathrm{T}}$$

$$\boldsymbol{\sigma} = \langle \sigma_{rr}, \sigma_{\theta\theta}, \sigma_{zz}, \tau_{rz}, \tau_{r\theta}, \tau_{\theta z} \rangle^{\mathrm{T}}$$

$$\Delta = \begin{bmatrix} \dfrac{\partial}{\partial r} & 0 & 0 \\ \dfrac{1}{r} & 0 & -\dfrac{n}{r} \\ 0 & \dfrac{\partial}{\partial z} & 0 \\ \dfrac{\partial}{\partial z} & \dfrac{\partial}{\partial r} & 0 \\ \dfrac{n}{r} & 0 & -\dfrac{1}{r}+\dfrac{\partial}{\partial r} \\ 0 & \dfrac{n}{r} & \dfrac{\partial}{\partial z} \end{bmatrix}$$

$$\mathbf{D} = \left[\begin{array}{ccc|c} D_{rr} & D_{r\theta} & D_{rz} & \\ D_{r\theta} & D_{rr} & D_{rz} & \mathbf{0} \\ D_{rz} & D_{rz} & D_{zz} & \\ \hline & & & G_{rz} \\ & \mathbf{0} & & G_{r\theta} \\ & & & G_{rz} \end{array}\right] \quad \text{where } G_{r\theta} = \frac{1}{2}(D_{rr} - D_{r\theta})$$

For an isotropic material, $D_{rr} = D_{zz} = \lambda + 2G$; $D_{r\theta} = D_{rz} = \lambda$; $G_{rz} = G_{r\theta} = G$ where λ = Lamé constant

$$\mathbf{L}_\sigma = \begin{bmatrix} \frac{1}{r}+\frac{\partial}{\partial r} & -\frac{1}{r} & 0 & \frac{\partial}{\partial z} & -\frac{n}{r} & 0 \\ 0 & 0 & \frac{\partial}{\partial z} & \frac{1}{r}+\frac{\partial}{\partial r} & 0 & -\frac{n}{r} \\ 0 & \frac{n}{r} & 0 & 0 & \frac{2}{r}+\frac{\partial}{\partial r} & \frac{\partial}{\partial z} \end{bmatrix}$$

$$\mathbf{H}^{(i)} = \begin{bmatrix} \frac{\mathrm{d}H_n^{(i)}}{\mathrm{d}r} & 0 & \frac{n}{r}H_n^{(i)} \\ 0 & kH_n^{(i)} & 0 \\ \frac{n}{r}H_n^{(i)} & 0 & \frac{\mathrm{d}H_n^{(i)}}{\mathrm{d}r} \end{bmatrix}$$

where $H_n^{(i)} = H_n^{(i)}(kr)$ is the Hankel function of the ith kind and nth order.

$$\mathbf{L} = \left[\begin{array}{c|c|c} k^2 D_{rr} - G_{rz}\frac{\mathrm{d}^2}{\mathrm{d}z^2} - G'_{rz}\frac{\mathrm{d}}{\mathrm{d}z} & -k(D_{rz}+G_{rz})\frac{\mathrm{d}}{\mathrm{d}z} - kG'_{rz} & 0 \\ \hline k(G_{rz}+D_{rz})\frac{\mathrm{d}}{\mathrm{d}z} + kD'_{rz} & k^2 G_{rz} - D_{zz}\frac{\mathrm{d}^2}{\mathrm{d}z^2} - D'_{zz}\frac{\mathrm{d}}{\mathrm{d}z} & 0 \\ \hline 0 & 0 & k^2 G_{r\theta} - G_{rz}\frac{\mathrm{d}^2}{\mathrm{d}z^2} - G'_{rz}\frac{\mathrm{d}}{\mathrm{d}z} \end{array}\right]$$

in which $(\quad)' = \dfrac{\mathrm{d}(\quad)}{\mathrm{d}z}$

$$\mathbf{L}_\mathrm{b} = \begin{bmatrix} -G_{rz}\frac{\mathrm{d}}{\mathrm{d}z} & -kG_{rz} & 0 \\ kD_{rz} & -D_{zz}\frac{\mathrm{d}}{\mathrm{d}z} & 0 \\ 0 & 0 & -G_{rz}\frac{\mathrm{d}}{\mathrm{d}z} \end{bmatrix}$$

$$\mathbf{L}_1 = \begin{bmatrix} k^2 D_{rr} & -kD_{rz}\frac{\mathrm{d}}{\mathrm{d}z} & 0 \\ kG_{rz}\frac{\mathrm{d}}{\mathrm{d}z} & k^2 G_{rz} & 0 \\ 0 & 0 & k^2 G_{r\theta} \end{bmatrix}$$

$$\mathbf{L}_2 = \begin{bmatrix} G_{rz}\dfrac{\mathrm{d}}{\mathrm{d}z} & kG_{rz} & 0 \\ -kD_{rz} & D_{zz}\dfrac{\mathrm{d}}{\mathrm{d}z} & 0 \\ 0 & 0 & G_{rz}\dfrac{\mathrm{d}}{\mathrm{d}z} \end{bmatrix}$$

Interpolation matrix for element l:

$$\mathbf{N}_l = \frac{1}{h_l}\begin{bmatrix} N_1 & N_2 & 0 & 0 & 0 & 0 \\ 0 & 0 & N_1 & N_2 & 0 & 0 \\ 0 & 0 & 0 & 0 & N_1 & N_2 \end{bmatrix}$$

where $h_l = \bar{z}_{l+1} - \bar{z}_l$; $N_1 = \bar{z}_{l+1} - z$; $N_2 = z - \bar{z}_l$

Rayleigh wave layer matrices (material constants are for layer l):

$$\mathbf{A}_{\mathrm{R},l} = \frac{h_l}{3}\left[\begin{array}{cc:cc} D_{rr} & \frac{1}{2}D_{rr} & \multicolumn{2}{c}{\multirow{2}{*}{$\mathbf{0}$}} \\ \frac{1}{2}D_{rr} & D_{rr} & & \\ \hdashline \multicolumn{2}{c:}{\multirow{2}{*}{$\mathbf{0}$}} & G_{rz} & \frac{1}{2}G_{rz} \\ & & \frac{1}{2}G_{rz} & G_{rz} \end{array}\right] = \left[\begin{array}{c:c} \mathbf{A}_{x,l} & \mathbf{0} \\ \hdashline \mathbf{0} & \mathbf{A}_{z,l} \end{array}\right]$$

$$\mathbf{B}_{\mathrm{R},l} = \left[\begin{array}{c:c} \mathbf{0} & \mathbf{B}_{xz,l} \\ \hdashline \mathbf{B}_{xz,l}^{\mathrm{T}} & \mathbf{0} \end{array}\right] \quad ; \quad \mathbf{B}_{xz,l} = \frac{1}{2}\left[\begin{array}{c:c} (D_{rz} - G_{rz}) & -(D_{rz} + G_{rz}) \\ \hdashline (D_{rz} + G_{rz}) & -(D_{rz} - G_{rz}) \end{array}\right]$$

$$\bar{\mathbf{C}}_{\mathrm{R},l} = \frac{1}{h_l}\left[\begin{array}{cc:cc} G_{rz} & -G_{rz} & \multicolumn{2}{c}{\multirow{2}{*}{$\mathbf{0}$}} \\ -G_{rz} & G_{rz} & & \\ \hdashline \multicolumn{2}{c:}{\multirow{2}{*}{$\mathbf{0}$}} & D_{zz} & -D_{zz} \\ & & -D_{zz} & D_{zz} \end{array}\right] = \left[\begin{array}{c:c} \bar{C}_{x,l} & \mathbf{0} \\ \hdashline \mathbf{0} & \bar{C}_{z,l} \end{array}\right]$$

$$\mathbf{M}_{\mathrm{R},l} = \frac{h_l \rho}{3}\left[\begin{array}{cc:cc} 1 & 1/2 & \multicolumn{2}{c}{\multirow{2}{*}{$\mathbf{0}$}} \\ 1/2 & 1 & & \\ \hdashline \multicolumn{2}{c:}{\multirow{2}{*}{$\mathbf{0}$}} & 1 & 1/2 \\ & & 1/2 & 1 \end{array}\right] = \left[\begin{array}{c:c} \mathbf{M}_l & \mathbf{0} \\ \hdashline \mathbf{0} & \mathbf{M}_l \end{array}\right]$$

$$\mathbf{C}_{\mathrm{R},l} = \bar{\mathbf{C}}_{\mathrm{R},l} - \omega^2 \mathbf{M}_{\mathrm{R},l}$$

Love wave layer matrices:

$$\mathbf{A}_{\mathrm{L},l} = \frac{G_{r\theta} h_l}{3}\begin{bmatrix} 1 & \frac{1}{2} \\ \frac{1}{2} & 1 \end{bmatrix}$$

$$\bar{\mathbf{C}}_{\mathrm{L},l} = \bar{\mathbf{C}}_{x,l}$$

$$\mathbf{M}_{\mathrm{L},l} = \mathbf{M}_l$$

$$\mathbf{C}_{\mathrm{L},l} = \bar{\mathbf{C}}_{x,l} - \omega^2 \mathbf{M}_l = \mathbf{C}_{x,l}$$

$$\mathbf{H}_{\mathrm{R}j} = \begin{bmatrix} \frac{\mathrm{d}}{\mathrm{d}r} H_n^{(2)}(k_{\mathrm{R}j} r) \cdot \mathbf{I}_m & \mathbf{0} \\ \mathbf{0} & k_j H_n^{(2)}(k_{\mathrm{R}j} r) \cdot \mathbf{I}_m \\ \frac{n}{r} H_n^{(2)}(k_{\mathrm{R}j} r) \cdot \mathbf{I}_m & \mathbf{0} \end{bmatrix}$$

$$\mathbf{H}_{\mathrm{L}j} = \begin{bmatrix} \frac{n}{r} H_n^{(2)}(k_{\mathrm{L}j} r) \cdot \mathbf{I}_m \\ \mathbf{0} \\ \frac{\mathrm{d}}{\mathrm{d}r} H_n^{(2)}(k_{\mathrm{L}j} r) \cdot \mathbf{I}_m \end{bmatrix}$$

where $\mathbf{I}_m$ is the $m \times m$ identity matrix.

APPENDIX II—ADDITIONAL SOLUTIONS

Point loads

The participation factors for unit point loads acting in or on a layered medium follow simply as the limiting value of the participation factors for ring loads, equations (26), if the magnitude of the load is held constant while the diameter of the ring is allowed to approach zero ($r_0 \to 0$). The resulting factors, which are to be used in conjunction with equations (25) to obtain displacements, are as follows:

Vertical point load ($n = 0$) at layer l:

$$\alpha_{\mathrm{R}j} = \frac{1}{2\pi} k_{\mathrm{R}j} Z_{lj}$$

$$\alpha_{\mathrm{L}j} = 0 \tag{A1}$$

Horizontal point load ($n = 1$) at layer l:

$$\alpha_{\mathrm{R}j} = \frac{1}{2\pi} k_{\mathrm{R}j} X_{lj}$$

$$\alpha_{\mathrm{L}j} = \frac{1}{2\pi} k_{\mathrm{L}j} Y_{lj} \tag{A2}$$

The solutions for point loads are useful for problems which require a full three-dimensional treatment. For example, a 3-D stiffness matrix of the soil can be easily computed and used in soil–structure interaction problems involving non-axisymmetric structures. Another application would be the study of wave propagation.

Line loads

The two-dimensional (plane strain) solutions for line loads can be obtained from the solutions for ring loads as the limiting case as $r_0, R \to \infty$. In this case the Hankel and Bessel functions can be replaced with their asymptotic expansions in terms of exponential functions. The displacements at a distance $x \geqslant 0$ away from the line loads are as follows:

$$\mathbf{u} = -\frac{1}{2} \sum_{j=1}^{2m} k_{\mathrm{R}j} \mathbf{x}_j \alpha_{\mathrm{R}j} \cdot \mathrm{e}^{-\mathrm{i}k_{\mathrm{R}j} x} \cdot \mathrm{e}^{\mathrm{i}\omega t} \tag{A3a}$$

$$\mathbf{w} = \frac{-\mathrm{i}}{2} \sum_{j=1}^{2m} k_{\mathrm{R}j} \mathbf{z}_j \alpha_{\mathrm{R}j} \cdot \mathrm{e}^{-\mathrm{i}k_{\mathrm{R}j} x} \cdot \mathrm{e}^{\mathrm{i}\omega t} \tag{A3b}$$

$$\mathbf{v} = \frac{-\mathrm{i}}{2} \sum_{j=1}^{2m} k_{\mathrm{L}j} \mathrm{y}_j \alpha_{\mathrm{L}j} \cdot \mathrm{e}^{-\mathrm{i}k_{\mathrm{L}j}x} \cdot \mathrm{e}^{\mathrm{i}\omega t} \tag{A3c}$$

The participation factors for the various line loads ($n = 0$) at layer l are:

Vertical line load, p_z:

$$\begin{aligned} \alpha_{\mathrm{R}j} &= Z_{lj} p_z \\ \alpha_{\mathrm{L}j} &= 0 \end{aligned} \tag{A4}$$

Horizontal line load, p_r:

$$\begin{aligned} \alpha_{\mathrm{R}j} &= \mathrm{i} X_{lj} p_r \\ \alpha_{\mathrm{L}j} &= 0 \end{aligned} \tag{A5}$$

Horizontal shearing line load, p_θ:

$$\begin{aligned} \alpha_{\mathrm{R}j} &= 0 \\ \alpha_{\mathrm{L}j} &= Y_{lj} p_\theta \end{aligned} \tag{A6}$$

Disk loads

Displacements caused by disk loads (distributed loads over a circular area) can be obtained by integrating the participation factors for ring loads along the radius of the loaded area. The layer boundary displacements at $r = R$ for four types of disk loading with radius r_0 are as follows.

Vertical disk load ($n = 0$) at layer l, constant load $p = p_z$:

$$\mathbf{u} = -\frac{\mathrm{i}\pi}{2} \sum_{j=1}^{2m} \mathrm{x}_j Z_{lj} p_z \cdot \begin{cases} r_0 H_0^{(2)'}(k_{\mathrm{R}j} R) J_1(k_{\mathrm{R}j} r_0) \\ r_0 J_0'(k_{\mathrm{R}j} R) H_1^{(2)}(k_{\mathrm{R}j} r_0) \end{cases} \cdot \mathrm{e}^{\mathrm{i}\omega t} \quad \begin{matrix} R \geqslant r_0 \\ R \leqslant r_0 \end{matrix} \tag{A7a}$$

$$\mathbf{w} = -\frac{\mathrm{i}\pi}{2} \sum_{j=1}^{2m} \mathrm{z}_j Z_{lj} p_z \cdot \begin{cases} k_{\mathrm{R}j} r_0 H_0^{(2)}(k_{\mathrm{R}j} R) J_1(k_{\mathrm{R}j} r_0) \\ k_{\mathrm{R}j} r_0 J_0(k_{\mathrm{R}j} R) H_1^{(2)}(k_{\mathrm{R}j} r_0) + \dfrac{2}{\mathrm{i}\pi} \end{cases} \cdot \mathrm{e}^{\mathrm{i}\omega t} \quad \begin{matrix} R \geqslant r_0 \\ R \leqslant r_0 \end{matrix} \tag{A7b}$$

$$\mathbf{v} = \mathbf{0} \tag{A7c}$$

Torsional disk load ($n = 0$) at layer l, $p = p_\theta \cdot \dfrac{r}{r_0}$ (linear variation):

$$\mathbf{u} = \mathbf{0} \tag{A8a}$$

$$\mathbf{w} = \mathbf{0} \tag{A8b}$$

$$\mathbf{v} = +\frac{\mathrm{i}\pi}{2} \sum_{j=1}^{m} \mathrm{y}_j Y_{lj} p_\theta \cdot \begin{cases} r_0 H_0^{(2)'}(k_{\mathrm{L}j} R) J_2(k_{\mathrm{L}j} r_0) \\ r_0 J_0'(k_{\mathrm{L}j} R) H_2^{(2)}(k_{\mathrm{L}j} r_0) - \dfrac{2R}{\mathrm{i}\pi r_0} \end{cases} \cdot \mathrm{e}^{\mathrm{i}\omega t} \quad \begin{matrix} R \geqslant r_0 \\ R \leqslant r_0 \end{matrix} \tag{A8c}$$

Horizontal disk load ($n = 1$) at layer l, constant load $p = p_r = p_\theta$ with $p_r \cdot \cos\theta$ and $-p_\theta \cdot \sin\theta$:

$$\mathbf{u} = -\frac{\mathrm{i}\pi}{2} \left[\sum_{j=1}^{2m} \mathrm{x}_j X_{lj} p \cdot \begin{cases} r_0 H_1^{(2)'}(k_{\mathrm{R}j} R) J_1(k_{\mathrm{R}j} r_0) \\ r_0 J_1'(k_{\mathrm{R}j} R) H_1^{(2)}(k_{\mathrm{R}j} r_0) + \dfrac{2}{\mathrm{i}\pi} \end{cases} \right.$$

$$\left. + \frac{1}{R} \sum_{j=1}^{m} \mathrm{y}_j Y_{lj} p \cdot \begin{cases} r_0 H_1^{(2)}(k_{Lj} R) J_1(k_{\mathrm{L}j} r_0) \\ r_0 J_1(k_{\mathrm{L}j} R) H_1^{(2)}(k_{\mathrm{L}j} r_0) \end{cases} \right] \cdot \cos\theta \cdot \mathrm{e}^{\mathrm{i}\omega t} \quad \begin{matrix} R \geqslant r_0 \\ R \leqslant r_0 \end{matrix} \tag{A9a}$$

$$w = -\frac{i\pi}{2}\sum_{j=1}^{2m} z_j X_{lj} k_{Rj} p \cdot \begin{cases} r_0 H_1^{(2)}(k_{Rj}R) J_1(k_{Rj}r_0) \\ r_0 J_1(k_{Rj}R) H_1^{(2)}(k_{Rj}r_0) \end{cases} \cdot \cos\theta \cdot e^{i\omega t} \quad \begin{matrix} R \geqslant r_0 \\ R \leqslant r_0 \end{matrix} \tag{A9b}$$

$$v = -\frac{i\pi}{2}\left[\frac{1}{R}\sum_{j=1}^{2m} x_j X_{lj} p \cdot \begin{cases} r_0 H_1^{(2)}(k_{Rj}R) J_1(k_{Rj}r_0) \\ r_0 J_1(k_{Rj}R) H_1^{(2)}(k_{Rj}r_0) \end{cases}\right.$$

$$\left. + \sum_{j=1}^{m} y_j Y_{lj} p \cdot \begin{cases} r_0 H_1^{(2)'}(k_{Lj}R) J_1(k_{Lj}r_0) \\ r_0 J_1'(k_{Lj}R) H_1^{(2)}(k_{Lj}r_0) + \dfrac{2}{i\pi} \end{cases}\right] \cdot (-\sin\theta) \cdot e^{i\omega t} \quad \begin{matrix} R \geqslant r_0 \\ R \leqslant r_0 \end{matrix} \tag{A9c}$$

Rocking disk load ($n = 1$) at layer l, $p = p_z \cdot r/r_0 \cos\theta$:

$$u = -\frac{i\pi}{2}\sum_{j=1}^{2m} x_j Z_{lj} p_z \cdot \begin{cases} r_0 H_1^{(2)'}(k_{Rj}R) J_2(k_{Rj}r_0) \\ r_0 J_1'(k_{Rj}R) H_2^{(2)}(k_{Rj}r_0) + \dfrac{2}{i\pi k_{Rj} r_0} \end{cases} \cdot \cos\theta \cdot e^{i\omega t} \quad \begin{matrix} R \geqslant r_0 \\ R \leqslant r_0 \end{matrix} \tag{A10a}$$

$$w = -\frac{i\pi}{2}\sum_{j=1}^{2m} z_j Z_{lj} p_z \cdot \begin{cases} k_{Rj} r_0 H_1^{(2)}(k_{Rj}R) J_2(k_{Rj}r_0) \\ k_{Rj} r_0 J_1(k_{Rj}R) H_2^{(2)}(k_{Rj}r_0) + \dfrac{2R}{i\pi r_0} \end{cases} \cdot \cos\theta \cdot e^{i\omega t} \quad \begin{matrix} R \geqslant r_0 \\ R \leqslant r_0 \end{matrix} \tag{A10b}$$

$$v = -\frac{i\pi}{2}\sum_{j=1}^{2m} x_j Z_{lj} p_z \cdot \begin{cases} \dfrac{r_0}{R} H_1^{(2)}(k_{Rj}R) J_2(k_{Rj}r_0) \\ \dfrac{r_0}{R} J_1(k_{Rj}R) H_2^{(2)}(k_{Rj}r_0) + \dfrac{2}{i\pi k_{Rj} r_0} \end{cases} \cdot (-\sin\theta) \cdot e^{i\omega t} \quad \begin{matrix} R \geqslant r_0 \\ R \leqslant r_0 \end{matrix} \tag{A10c}$$

Again, the prime indicates differentiation with respect to r. The expressions for the two regions $R \geqslant r_0$ and $R \leqslant r_0$ can be shown to be identical at $R = r_0$. The above solutions can be shown to be identical to Kausel's solutions[13] for the case of an isotropic medium.

REFERENCES

1. J. E. Luco and R. A. Westmann, 'Dynamic response of circular footings', *J. eng. mech. div. ASCE* **97**, 1381–1395 (1971).
2. A. S. Veletsos and Y. T. Wei, 'Lateral and rocking vibration of footings', *Report No. 8*, Department of Civil Engineering, Rice University, Houston, TX, 1971.
3. J. E. Luco, 'Vibrations of a rigid disk on a layered viscoelastic medium', *Nuc. eng. des.* **36**, 325–340 (1976).
4. R. J. Apsel and J. E. Luco, 'Torsional response of rigid embedded foundation', *J. eng. mech. div. ASCE* **102**, 957–970 (1976)
5. V. W. Lee and M. D. Trifunac, 'Body wave excitation of embedded hemisphere', *J. eng. mech. div. ASCE* **108**, 546–563 (198
6. G. Dasgupta, 'Foundation impedance matrices by substructure deletion', *J. eng. mech. div. ASCE* **106**, 517–523 (1980).
7. J. P. Wolf and G. R. Darbre, 'Dynamic-stiffness matrix of soil by the boundary-element method: conceptual aspects', *Earthquake eng. struct. dyn.* **12**, 385–400 (1984).
8. J. P. Wolf and G. R. Darbre, 'Dynamic-stiffness matrix of soil by the boundary-element method: embedded foundation', *Earthquake eng. struct. dyn.* **12**, 401–416 (1984).
9. G. Waas, 'Dynamisch belastete Fundamente auf geschichtetem Baugrund', *VDI-Berichte* No. 381, 185–191 (1980).
10. G. Waas and H.-G. Hartmann, 'Analysis of pile foundations under dynamic loads', *SMiRT 6*, Paris (1981) Paper K5/2.
11. G. Waas and H. Werkle, 'Response of nuclear power plant structures to the air pressure wave and the induced ground wave caused by gas explosions similar to detonations, part 2: induced ground wave', Hochtief AG, Abt. KTI, under contract to Bundesministerium für Forschung und Technologie, December 1982 (in German).
12. H. Tajimi, 'A contribution to theoretical prediction of dynamic stiffness of surface foundations', *Proc. 7th world conf. earthquake eng.*, Istanbul **5**, 105–112 (1980).
13. E. Kausel, 'An explicit solution for the Green functions for dynamic loads in layered media', *Report R81-13*, with *Errata, No. 699*, Department of Civil Engineering, MIT, Cambridge, Mass., 1981.
14. E. Kausel and R. Peek, 'Dynamic loads in the interior of a layered stratum: an explicit solution', *Bull. seism. soc. Am.* **72**, 1459–1481 (1982).
15. J. Lysmer and G. Waas, 'Shear waves in plane infinite structures', *J. eng. mech. div. ASCE* **98**, 85–105 (1972).
16. G. Waas, 'Analysis method for footing vibrations through layered media', *Tech. Report S-71-14*, No. 3, U.S. Engineer Waterways Experiment Station, Vicksburg, Miss., 1972; also 'Linear two-dimensional analysis of soil dynamics problems in semi-infinite layered media', Dissertation, University of California, Berkeley, 1972.

17. E. Kausel, 'Forced vibrations of circular foundations on layered media', *Report R74-11, Soils Publication No. 336*, Department of Civil Engineering, MIT, Cambridge, Mass., 1974.
18. E. Kausel, J. M. Roesset and G. Waas, 'Dynamic analysis of footings on layered media', *J. eng. mech. div. ASCE* **101**, 679–693 (1975).
19. K. Sezawa, 'Further studies on Rayleigh-waves having some azimuthal distribution', *Bull. earthquake res. inst.* **6**, 1–18 (1929).
20. E. Kausel and R. Ushijima, 'Vertical and torsional stiffness of cylindrical footings', *Report R79-6*, Department of Civil Engineering, MIT, Cambridge, Mass., 1979.
21. F. Elsabee and J. P. Morray, 'Dynamic behaviour of embedded foundations', *Report R77-3*, Department of Civil Engineering, MIT, Cambridge, Mass., 1977.
22. D. J. Kirkner, 'Vibration of a rigid disk on a transversely isotropic elastic half space', *Int. jour. numer. methods geomech.* **6**, 293–306 (1982).
23. G. Waas and H. R. Riggs, 'Effect of the flexibility of the base mat on seismic response of a PWR-reactor building', *SMiRT 7*, Chicago (1983), Paper K 8/8.
24. G. Waas, 'Berechnung dynamischer Boden-Bauwerk-Wechselwirkungen', *Proc. Finite Elemente-Anwendung in der Baupraxis*, Munich, to be published by Wilhelm Ernst & Sohn, 1984.
25. H. Werkle and G. Waas, 'Ground waves caused by gas cloud explosions and their effect on nuclear power plant structures', *SMiRT 7*, Chicago (1983), Paper J 10/4.
26. H. Werkle, 'Kinematic interaction of rigid circular foundations on layered soil under surface wave excitation', *Proc. 8WCEE*, San Francisco (1984), **3**, 945–952.